The 5th IEEE International Workshop on Performance and Management of Wireless and Mobile Networks (P2MNET 2009)
Zürich, Switzerland; 20-23 October 2009

Improving Radiation Oncology Using a Low-Cost Wireless Accelerometer

Farid Farahmand[1], K. O. Khadivi[2], and Joel J. P. C. Rodrigues[3]

[1]Department of Engineering Science, Sonoma State University, CA 94928, USA
[2]Austin Cancer Center, 2600 E. Martin Luther King Jr. Blvd., Austin, Texas 78702, USA
[3] Instituto de Telecomunicações, University of Beira Interior, 6201-001 Covilhã, Portugal
Emails: *farid.farahmand@sonoma.edu; bepish@flash.net; joeljr@ieee.org*

Abstract— **Born on military applications, wireless sensor networks span over to different application fields, namely on eHealth and medical applications. In this paper we discuss a high-precision, non-intrusive, wireless, accelerometer-based patient movement monitoring system (APMMS) in determining positional change in patients undergoing radiation treatment. Using this system a small wireless accelerometer sensor is placed on patient's skin, broadcasting its precise position to the receiving station connected to a PC in the control area. A threshold-based algorithm is developed to identify the exact amount of patient's movement and its direction. Our results indicate that, in spite of its low-cost and simplicity, APMMS is highly sensitive and offers accurate measurements.**

Index Terms— **Position Monitoring System, Wireless Sensor Networks, Body Sensor Networks.**

I. INTRODUCTION

ADVANCES in wireless sensor networks (WSN) have created many new opportunities in healthcare and medical systems. Examples of WSN applications in such areas are monitoring blood pressure and oxygenation, breathing, heart rate, heart rhythm, electroencephalogram (EEG), and electrocardiogram (ECG). Wireless sensor networks have also been considered for high-precision, non-intrusive, position monitoring.

Patient position monitoring is particularly essential for accurately delivered radiation therapy treatments, especially in brain tumor patients. With the advent of Stereotactic Radiation Therapy (SRT) and ever decreasing target margins, even a nearly imperceptible movement may have a substantial negative impact on a patient's outcome. Vigilant active observation of patient movement serves two primary purposes: (1) it ensures that a patient who inadvertently moves during treatment will not receive improperly directed dose; (2) it ensures that radiation is properly delivered in spite of involuntary patient movements, e.g., breathing [1].

Although considerable efforts are often undertaken to properly immobilize a patient, in many situations complete immobilization is not used or not possible. Even when stringent immobilization precautions are taken, patient movement caused by physiological behaviors is generally extremely difficult, if not impossible, to prevent [2] - [3]. Similar studies have demonstrated that the problem is even more pronounced when patients are not thoroughly immobilized [4] - [5]. Despite such difficulties, few accurate patient position monitoring systems currently exist. A passive visual monitoring by radiation therapists, using video cameras in the treatment room, is the prevalent conventional method. More advanced options are currently available, yet these methods are generally expensive and cumbersome, with a somewhat limited function.

In this preliminary study, we report our efforts in developing a wireless accelerometer-based patient motion monitoring system (APMMS). The developed system is low-cost, low-power, small, and reusable and it has a highly flexible software platform. Hence, it can potentially overcome many of the drawbacks associated with existing movement monitoring systems. Instead of imaging and calculating the movement of a small fiducial positioned on a patient, as is commonly utilized, APMMS can be directly attached to the patient to report change in position without any imaging by ionizing radiation. The accelerometer sensor in APMMS has the capability to detect sub-degree rotation in all three orthogonal directions. The number of sensors can easily be expended in order to simultaneously monitor movement of multiple body locations. Our test results indicate that in addition to being highly accurate and sensitive, APMMS can perform well under high energy radiation conditions. Furthermore, while APMMS provides sufficient signal strength for wireless communications, it does not interfere with radiation delivery.

The remainder of this paper is structured as follow. In Section 2, we describe a typical clinical treatment environment. In Section 3, we elaborate on hardware description. In Section 4, we present details of the signal processing algorithm. In Section 5, we provide a general overview of the software implementation. Finally, in Section 6, we characterize the performance of APMMS, followed by concluding remarks.

II. Clinical Treatment Environment

In this section we briefly describe the general setup used in a typical X-ray or radiation oncology (cancer therapy) procedure.

Figure 1(a) depicts a typical brain cancer therapy treatment. The collimator, mounted on top of the gantry in the linear accelerator (linac), delivers radiation in a pre-determined pattern to the target. The APMMS consists of two parts: the wireless node (WN) and the base station (BS). The accelerometer sensor of the wireless node is attached to the patient in the treatment room, as shown in Figure 1(a). The base station is placed in the control room for monitoring the patients' movements. As shown in Figure 1(a), the control room and the treatment room are completely isolated with a thick shield wall. The shielding structure has a very high attenuation factor and it is designed to prevent personnel access and limiting exposure to scattered radiation from the collimator. The total distance between the RF antenna of the WN and the BS is equivalent to $d_1 + d_2 + d_3$, as shown in Figure 1(a).

Figure 1(b) shows biodynamic coordinate system for human head[1]. In this Figure 1 *g* displacement (90 degree rotation) is equivalent to the gravitational attraction that the Earth exerts on objects (e.g., the head) or near its surface, and it is approximately 9.80665 m/s² or 32.1740 ft/s². As shown in the figure, the accelerometer sensor and the radiation target are separated by distance *R*. We call this the *exposure distance*. Location of the sensor and selection of *R* value must be such that any patient's movement, resulting in displacement of the radiation target, can be accurately monitored and measured. In this figure we assume the accelerometer of the WN is attached to the chin of the patient.

III. Hardware Description

Figure 2 depicts the main hardware components of APMMS prototype. The small (4x4x1.45 mm) accelerometer, mounted on a breadboard (2x2 cm), is attached to the patient's body. The wireless communication between the accelerometer and the base station is supported by Xbee transceiver [13].

Figure 2(a) shows the two main components of APMMS: WN and BS. In the following paragraphs we describe the functionality of each component in details.

A. Wireless Node (WN)

The WN consists of two separate parts wired together: the accelerometer sensor and the Xbee transceiver. The sensor is a small, low-g, low-power iMEMS accelerometer from Analog Devices (ADXL330) [6], shown in Figure 2(b). An accelerometer can measure both dynamic and static change of acceleration. The device is a polysilicon surface micromachined structure built on top of a silicon wafer [11].

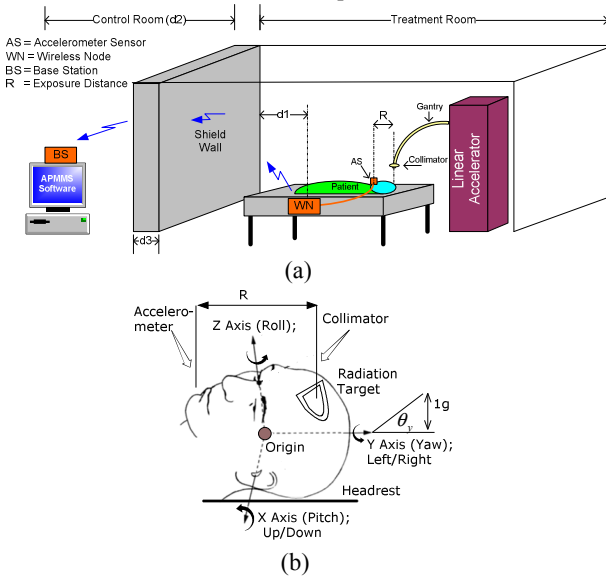

Figure 1: (a) Radiation treatment setup using the linear accelerator; (b) head coordinates.

When the structure moves, the dynamic changes of acceleration in all directions are detected using independent X, Y, and Z axes. Each axis reports the recent magnitude of acceleration using an analog voltage. The voltage is converted to an equivalent g value, which can be used to calculate the tilt angle. Consequently, the choice of accelerometer was based on its ability to achieve high degree resolution of tilt measurement and sensitivity within a measurement range of (+/-) 3g.

The outputs of the accelerometer are directed to three of 10-bit analog-to-digital converter units on the XBee module, shown in Figure 2(c). The corresponding digital data is sent to the OEM RF module providing wireless data communication over ZigBee/802.15.4 protocol [9]. Hence, XBee modules operate in the license-free 2.4 GHz ISM band with a RF data rate of 250 Kbps.

With the receiver sensitivity of -97 dBm, the typical transmission range of a Xbee module can be adjusted for 30-120 meters. Using XBee 802.15.4 the transmit power output can be boosted as high as 60 mW (+18 dBm). Each XBee module comes in regular or long-range "–PRO" versions. In our design we used the PRO version to ensure maximum penetration through the shield wall.

The Xbee module can be configured using a series of AT commands. More advanced features, such as supporting multi-node topology, data transmission, data reception, etc, can be configured using APIs (application programming interface). The configuration can be performed locally or over the air. In our design we implemented point-to-point configuration between WN and BS. The wireless node is powered by two AA batteries at about 3.3V. For best performance, it is important to use fully charged batteries.

[1] ISO-8727 defines the biodynamic coordinate system for human head. In this paper we reference roll, pitch, and yaw to Z, X, and Y coordinates, respectively, which are base on accelerometers' coordinates.

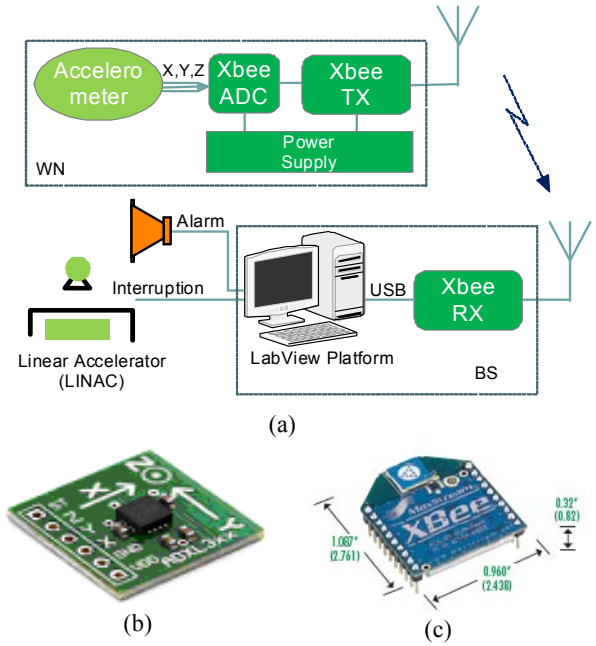

Figure 2: (a) Basic block diagram of APMMS; (b) ADXL330 accelerometer mounted on the breakout board, (c) Xbee transceiver.

B. *Base Station (BS)*

The base station consists of an Xbee transceiver connected to a PC. The Xbee transceiver directs the received digital data from the wireless node and passes it onto the PC via a USB interface. Using our own developed software, the received data is analyzed and displayed. As shown in Figure 2(a), the BS can be interfaced to the linear accelerometer and an audible alarm for notifying technicians of any undesired patient movement.

An important consideration in configuring the BS is properly setting its sensitivity. The receiver sensitivity of XBee can be set to as low as -100 dBm. The following expression shows the relation between the receiver sensitivity in dBm (Φ_{dBm}) and the transmitting power of the WN:

$$\Phi_{dBm} = 10\log[P_{tx} \cdot [\alpha_o(d_1 + d_2) + \alpha_{sh}(d_3)]], \quad (1)$$

where

$$\alpha_o(d_1 + d_2) = [4\pi \cdot (d_1 + d_2) \cdot f / C]^2. \quad (2)$$

In the above expressions P_{tx} is WN's transmitted power in mW, α_{sh} is the attenuation factor of the shield wall as a function of its thickness (d_3) defined in [8], and α_o is the free-space attenuation with d_1 and d_2 being the distance between the shield wall and WN and BS, respectively. This is shown in Figure 1(a). In Equation (2), C is the speed of light in free-space and f represents the license-free 2.4 GHz ISM band.

IV. Signal Processing Algorithm

The received data from the accelerometer must be properly filtered and interpreted in order to accurately identify patient's position. The signal processing algorithm constantly samples the accelerometer for static tilt information.

Figure 3 depicts the flowchart for the signal processing algorithm. Initially, the received data from the accelerometer must be converted to tilt angle using the following expressions:

$$\theta_{\deg} = \sin^{-1}\frac{(V_{measured} - V_{offset})}{\varphi}, \quad (3)$$

or

$$\theta_{rad} = \frac{\pi}{180}\sin^{-1}\frac{(V_{measured} - V_{offset})}{\varphi}; \quad (4)$$

where φ represents accelerometer's sensitivity in mV/g. Furthermore, $V_{measured}$ is the accelerometer reading in mV. The value of V_{offset} indicates the accelerometer's zero g offset. In our application values of V_{offset} for each axis were found independently. Note that the sign of θ determines the direction of the tilt (e.g., up/down or left/right). Using equation (3), for tilt angle of zero degree (zero g) $V_{measured} = V_{offset}$. The sensitivity value can be obtained from taking the difference between the measured values from the accelerometer at zero and 90 degrees, corresponding to zero and one g. Hence, the sensitivity can be calculated as follow:

$$\varphi = \frac{\Delta V}{\Delta g} = V_{measured}(g = 1) - V_{measuredt}(g = 0) \cdot \quad (5)$$

Using the above expressions, with a measured sensitivity value of 270 mV/g and having 10-bit ADC embedded in the Xbee transceiver powered by a 3.3 V power supply, it can be demonstrated that APMMS can accurately offer 0.23 degree resolution at zero degree. Lower resolution is expected as the value of g increases.

The received raw data from WN is sampled at a rate of 200 Hz. This sampling rate is sufficient to detect any sudden movement of the patient. However, the accelerometer is susceptible to noise. In order to ensure filtering the erroneous values measured by the accelerometer, the signal processing algorithm computes a running average to record the mean measured raw data over a period of one second. The choice of one second time interval was tested to be a good compromise between accurately obtaining data, while quickly detecting any changes in patient's position. The latest average tilt value is calculated using the following expression:

$$\bar{\theta}_s = \frac{\sum_{i=s}^{1}(\theta_i - \theta_{i-1})}{s}, \qquad (6)$$

where s is the data sampling rate (200 samples per second). In the above equation, $\bar{\theta}_s$ and $\bar{\theta}_1$ represent the latest and the first recorded (displayed) title angle, respectively, in the running average window. The running root-mean-square (rms) average of $\bar{\theta}_s$ for all three axes is also computed using

$$\bar{\theta}_{rms}(xyz) = \sqrt{\bar{\theta}(x)^2 + \bar{\theta}(y)^2 + \bar{\theta}(z)^2}\ . \qquad (7)$$

As shown in Figure 3, each average tilt value, including the rms average, is compared with the previous value to detect any change of position. Additional tolerance limits, θ_{th}, can be assigned to each axis for allowing a small acceptable displacement. Consequently, having $\bar{\theta}_s > \bar{\theta}_{s-1} - \theta_{th}$ indicates the patient moving in positive direction, where as having $\bar{\theta}_s < \bar{\theta}_{s-1} - \theta_{th}$, represents a movement in the negative direction. Under either condition, the interrupt circuitry and/or the alarm can be activated.

V. Software Implementation

Various software interfaces can be implemented to communicate with the Xbee module and process the signals from the accelerometer. In our prototype, we used LabVIEW programming language [10] for its ease of programming and versatility in data acquisition.

LabVIEW is a graphical program development application developed by National Instruments. LabVIEW program consists of two parts: the control panel, providing the graphical user interface (GUI) and the block diagram, containing all the programming codes.

Figure 4 shows the control panel designed for the APMMS. In this figure we only depict X- and Y-axis monitors due to space limitation.

Upon pressing the Lock button on the control panel, the user enables a reference position (e.g., $\theta^o(x)$) desired for radiation. For each independent axis a (+/-) tolerance limit can be assigned, allowing the patient limited flexibility in movement when undergoing radiation therapy. If the patient moves beyond either one of the tolerance limits, $\theta^o(x) \pm \theta_{th}(x)$, the alarm indicator button Radiation in Progress will be activated and an optional audible alarm can be set off. The selection of the tolerance limits for each axis depends on the accuracy of the dosimetric and radiation therapy procedure.

Figure 4 also shows the directional indicators on the control panel, identifying the direction of the patient's movement (e.g., right/left and up/down). This information can be used for repositioning the patient.

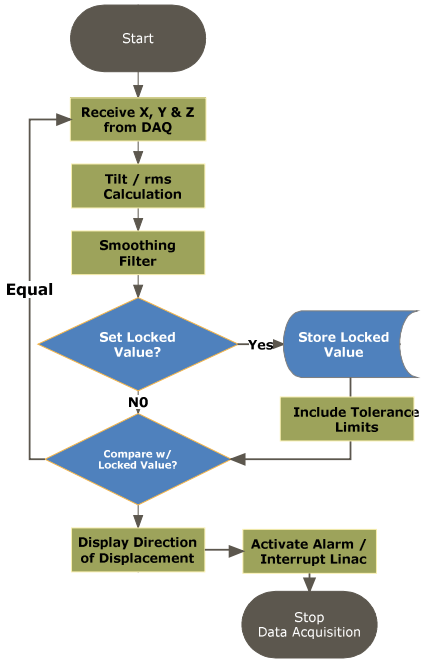

Figure 3: Flowchart of the signal processing algorithm used in APMMS.

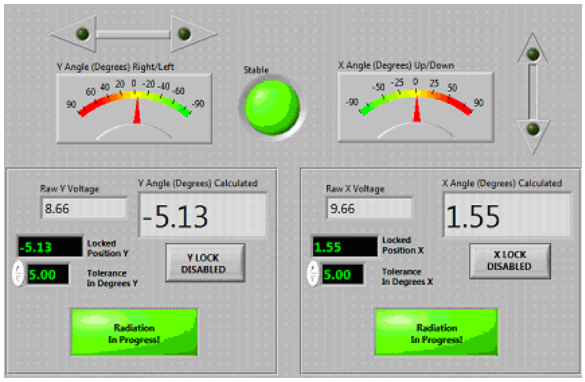

Figure 4: Control panel of APMMS using LabVIEW platform depicting monitors for only two axes.

VI. Experimental Setup and Results

In order to characterize the accelerometer, we mounted the WN on a Flexiholder [7]. Flexiholder allows moving a small platform in three dimensions. Each individual axis was tested independently. The data sampling rate and the moving average filter were set to 200 Hz and one sample per second, respectively. Each experiment was repeated multiple times to guarantee that the mean results a confidence interval of 15% or better at 90% confidence level. All reported results are referenced to X-, Y-, Z-axis of the accelerometer, as shown in Figure 2(b).

Figure 5 depicts a typical readout of APMMS, while monitoring a patient for a brief period of time after the system is locked to a reference position. The figure shows that the patient slightly moves her head followed by an inadvertent displacement from the reference position. Figure 6 shows

$\bar{\theta}(xyz)_{rms}$ for the same scenario. Note that previous to the sudden displacement, the patients' movements were within the tolerance limits from the reference position. When the displacement exceeds the threshold (e.g., $\theta^o \pm \theta_{th}$) the alarm is activated.

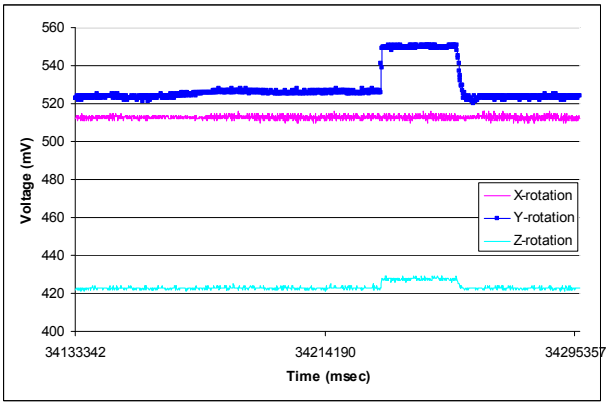

Figure 5: APMMS reading for all three axes.

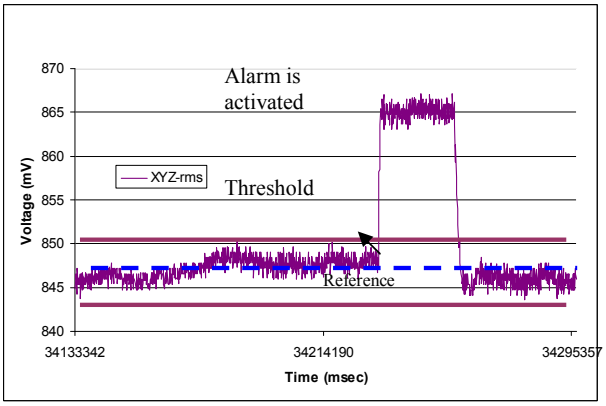

Figure 6: $\bar{\theta}(xyz)_{rms}$ during a typical treatment session.

The sensitivity and repeatability of APMMS in X-axis are demonstrated in Figure 7. Similar results can be achieved for Y- and Z-axis. For practical purposes, we only tested the changes within 15 degrees. The Min. and Max. values represent the lowest and highest values recorded. These results show that as the tilt angle increases, slightly larger variations from the mean are observed. This is due to the nonlinearity of the accelerometer's output. Hence, the accelerometer is most sensitive when the sensing axis is closer to zero degrees (zero g), and less sensitive when closer to 90 degrees (one g).

The performance of the moving average filter is shown in Figure 8. In this case the WN remained stationary for about one minute and raw data before and after the smoothing filter are recorded. This figure suggests that the X-axis of the accelerometer appears to be noisier than the other two axes. According to our results, the maximum reading variation in X-axis is about 5 mV, corresponding to about half degree, when having a 3.3 V power supply. In general, the noise density increases as the supply voltage drops. Hence, as the system operates for longer period of time, higher noise density is expected. For example, for ADXL330 accelerometer, the noise density at 3.6 V and 2V are reported to be 230 and 350 $\mu g\sqrt{Hz}$, respectively [6]. Hence, it is important to have WN's batteries fully charged prior to usage.

Actual	Mean Measured	Max. Measured	Min. Measured
0	0	0.3	0
3	3.1	3.5	2.7
6	6.2	6.3	5.8
9	9.2	9.4	8.4
12	12.3	12.7	11.3
15	15.2	15.8	14.8
12	12.3	12.5	11.5
9	9.3	9.4	8.7
6	6.3	6.3	6
3	3.2	3.5	3.1
0	0.1	0.2	0.1

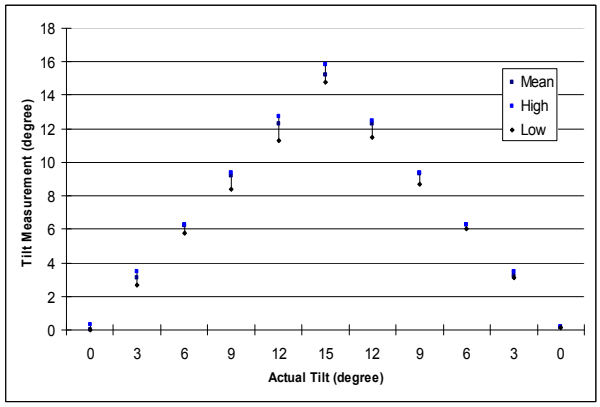

Figure 7: Tabulated comparison between the measured and actual tilt values in degrees for X-axis. Graphical representation of the points is also shown.

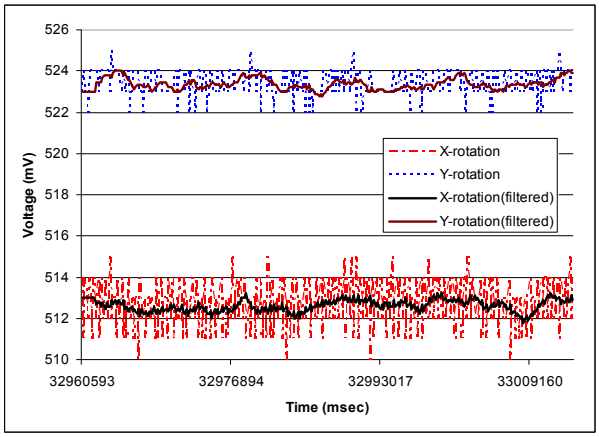

Figure 8: X- and Y-axis readings when the accelerometer is stationary with and without the smoothing filter.

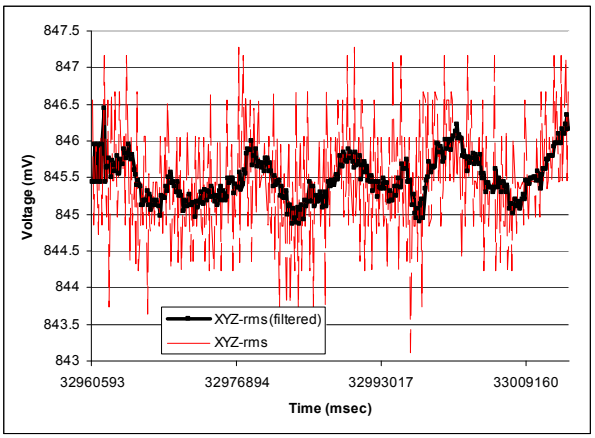

Figure 9: Calculated rms when the accelerometer is stationary with and without the smoothing filter.

Figure 9 compares the rms value of raw and filtered readings for the same scenario. This figure demonstrates that having the moving average filter can significantly reduce the erroneous readings reported by the accelerometer due to noise density and noise voltage in the power supply. Similar results were obtained when we extended the duration of testing to 10 minutes, which is equivalent to a typical radiation therapy session.

In order to fully verify the performance of APMMS, we tested it when the linear accelerator was activated. We examined the impact of the high energy X-ray source on the amount of noise generated on Xbee's RF signal. Our results suggest that the scattered radiation through the collimator radiating 15 MV[2], does not have any significant impact on WN's Xbee transceiver performance when it is kept about 30 cm away from the radiation target. Further study may be needed to characterize such distance in more details.

A major issue in APMMS's performance was found to be the significant attenuation of Xbee's RF signal through the shield wall that is designed to block the radiation leakage. The standard shield wall for CT scanning (also referred to as CAT scanning - Computerized Axial Tomography) with the source generating as high as 15 MV radiation is made of lead-borated-polyethylene and cement with high attenuation factor, depending on the wall's thickness. Consequently, using equation (1), for maximum performance, it is necessary to configure the transmission strength of Xbee-PRO for outdoor mode.

VII. Conclusions

In this paper we reported the utility of a low-cost, high-precision, real-time wireless accelerometer-based patient movement monitoring sensor (APMMS) in verifying positional change in patients undergoing radiation treatment. Important advantageous features of APMMS include ease of use on patients, requiring minimal user training, and needing no change in the typical patient setup.

[2] In this paper we use megavoltage (MV) X-Ray, referring to photon beams.

The design of APMMS is highly flexible. For example, it can be connected to multiple accelerometers, allowing detection of the position change in different parts of the patient's body, and hence, enabling a more complete data set to correlate the pattern of motion of the internal and external markers. In addition to detecting small, inadvertent patient movements, APMMS can be used in conjunction with different imaging modalities to function in a manner similar to available dynamic tumor tracking systems. For example, APMMS may be readily used with the Fluroscopy mode of an IGRT-capable linear accelerometer.

Our preliminary clinical test results indicate that APMMS is highly reliable and can accurately report sub-degree rotational displacements. More detailed clinical studies are required to quantify the system's efficacy and practicality in a simulated environment.

Acknowledgments

The authors would like to thank Mr. Mark Lynch, Mr. Leela Mohan Kesireddy, and Ms. Ivonne Mejia for their invaluable assistance in this project. Part of this work has been supported by the *Instituto de Telecomunicações*, NetGNA Group, Portugal, and by the Euro-NF Network of Excellence from the Seventh Framework Program of EU.

References

[1] J. Y. Jin, et al., "A Technique of Quantitatively Monitoring Both Respiratory and Nonrespiratory Motion in Patients Using External Body Markers," Med Phys. 2007; 34(7): 2875-2881.

[2] C . Dickie-Euler et al., "Measuring Interfraction and Intrafraction Motion with Cone Beam Computed Tomography (CBCT) and an Optical Localization System (OLS) for Lower Extremity Soft Tissue Sarcoma Patients Treated with Preoperative Intensity Modulated Radiation Therapy (IMRT)," International Journal of Radiation OncologyBiologyPhysic, Volume 72 , Issue 1, Pages S105 - S105 C .

[3] S Senthilkumar and V. Ramakrishnan; "In-house auto cutoff sensor device for radiotherapy machine to monitor patient movements," Journal of Applied Clinical Medical Physics, Volume 9, No 3 (2008).

[4] N. Lee, et al., "Intra-fraction patient motion in head/neck cancer patients undergoing intensity-modulated radiation therapy (IMRT)", International Journal of Radiation Oncology Biology Physics, Volume 57 , Issue 2 , Page S409, Oct. 2003.

[5] Manuel Bandala et al, "Tracking of internal organ motion with a six degree-of-freedom MEMS sensor: concept and simulation study," 2008 Meas. Sci. Technol. 19 024006. Retrieved on December 29, 2008, from http://www.iop.org/EJ/abstract/0957-0233/19/2/024006.

[6] Analog Devices, Inc. (2007). Small, Low Power, 3-Axis ±3 g iMEMS® Accelerometer. Retrieved October 6, 2008 from http://www.analog.com/static/imported-files/data_sheets/ADXL330.pdf.

[7] Huestis Medical, retrieved on December 29, 2008 from http://www.huestis.com/HuestisMed/prod_fhpgs/fh_features.html .

[8] Structural Shielding Design for Medical Imaging X-ray Facilities (NCRP Report No 147) G J Chalmers 2005 Phys. Med. Biol. 50 4243-4244.

[9] ZigBee Alliance, http://www.zigbee.org/en/index.asp.

[10] L. K. Wells and J. Travis, LabVIEW for everyone: graphical programming made even easier. 1996 - Prentice-Hall, Inc. Upper Saddle River, NJ, USA.

[11] M. Clifford and L. Gomez, "Measuring Tilt with Low-g Accelerometers," 2007, pp. 8, 05/2005. 2005. Retrieved October 6, 2008 from http://www.freescale.com/files/sensors/doc/app_note/AN3107.pdf.

[12] National Instruments. (2008). Low-Cost, Bus-Powered Multifunction DAQ for USB. Retrieved October 6, 2008 from http://www.ni.com/pdf/products/us/20043762301101dlr.pdf.

[13] XBee® & XBee-PRO RF Modules. Retrieved on December 28 from http://www.digi.com/products/wireless/zigbee-mesh/.